DOI: 10.61782/fa.2025.0088

FORUM ACUSTICUM EURONOISE 2025

ACOUSTIC RESONANCE SPECTROSCOPY USING FBG SENSORS EMBEDDED IN MORTARS

J. Gosalbez [1*] **V. J. Ruiz** [1] **J. Madrigal** [1]
A. M. Macián [2] **J. E. Carcel**[1] **J. Payá**[2]

[1] Inst. de Telecomunicaciones y Aplicaciones Multimedia. Universitat Politècnica de València. Spain
[2] Instituto de Ciencia y Tecnología del Hormigón, Universitat Politècnica de València. Spain

ABSTRACT

The high sensitivity of nonlinear terms in the elastic response of materials to the early appearance of damage has led to the emergence of the so-called NEWS methods (Non-linear Elastic Wave Spectroscopy). These NDE (Non-Destructive Evaluation) methods exploit the increase in the material's nonlinear behaviour as damage increases. In particular, the NIRAS technique (Non-linear Impact Resonance Acoustic Spectroscopy) detects changes in the resonance of a material (frequency, damping factor, etc.) as a function of impact intensity.
In this work, the NIRAS technique was employed to characterize damage in mortar concrete samples embedded with FBG (Fiber Bragg Grating) sensors. The advantage of this technique lies in the fact that these sensors can be integrated during the fabrication process, spatially distributed, share the same optical fiber, and be interrogated remotely.

Keywords: *impact resonance acoustic spectroscopy, thermal shock damage, fiber bragg grating sensors, thermal shock mortar degradation*

1. INTRODUCTION

Geomaterials—such as rocks, sand, soil, and combinations thereof like concrete—are classified within a specific group known as Non-Linear Mesoscopic Elastic (NME) materials [1]. These materials are characterized by their heterogeneous internal makeup, with a complex non-linear response strongly influenced by various microstructural elements, including micro-cracks, grain contacts, and voids. Compared to traditional atomic elastic materials, this response is significantly more pronounced. Due to these unique properties, the non-linear behavior of NME materials cannot be adequately described by Landau's classical non-linear elasticity theory [2].

One of the most effective methodologies for evaluating damage in concrete and other cementitious materials is the non-destructive technique known as Nonlinear Elastic Wave Spectroscopy (NEWS). This method focuses on analyzing various nonlinear phenomena [3], including the generation of higher-order harmonics, wave cross-modulation, shifts in resonance frequency, and amplitude-dependent attenuation. Despite variations in technique, all NEWS approaches share a common goal: to quantify non-linear material behaviors through dynamic responses.

Within the field of NEWS, impact spectroscopy has gained traction due to its straightforward excitation requirements and high sensitivity to non-linear effects. A notable example is the Non-linear Impact Resonance Acoustic Spectroscopy (NIRAS) technique. NIRAS operates by monitoring how the material's resonance frequency varies with different levels of impact force (see Figure 1), providing insights into internal structural changes.

Concrete degradation has been extensively studied over time, with research highlighting that different deterioration mechanisms alter their dynamic properties in distinct ways [4][5]. Concrete exposed to thermal shock (rapid

*Corresponding author: jorgocas@dcom.upv.es

temperature changes) can suffer significant internal damage due to the differential expansion and contraction of its constituent materials. This abrupt thermal gradient induces high tensile stresses, particularly at the interfaces between aggregates and the cement paste, often leading to microcracking, debonding, and eventual loss of mechanical integrity. Repeated thermal shocks can accelerate degradation, reducing stiffness, strength, and durability over time [6]. Investigations have applied NEWS techniques to evaluate thermal shock effects on concrete across various compositions and number of cycles [7][8] and changes in acoustic non-lineartity ybder thermal stress [9][10][11] [12].

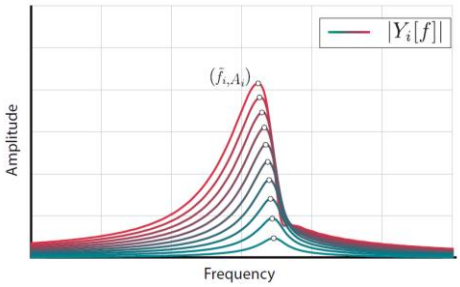

Figure 1. Received frequential response for the different impact levels ($Y_i(f)$)

In this study, the authors focus on the application of the NIRAS technique to evaluate thermal shock damage in mortar specimens, using embedded Fiber Bragg Gratings (FBGs) as sensors during the fabrication process. A key innovation lies in the simultaneous interrogation of multiple spatially separated FBG sensors inscribed along the same optical fiber. The performance of these FBG sensors is compared against that of surface-mounted accelerometers. While accelerometers are effective for measuring acceleration and vibration during impact events, FBGs offer precise strain and displacement measurements. Additionally, FBGs can be embedded within the material for long-term, remote monitoring and allow for the integration of multiple sensing points on a single fiber, enhancing spatial resolution.

2. MATHEMATICAL BACKGROUND

NIRAS is a method used for impact assessment and damage detection and involves impacting the material with different strength levels and analyzing the resulting acoustic frequency responses. The different reverberation signals are denoted by $y_i(t)$ where i denotes the different impacts and $Y_i(f)$ is the Fourier Transform of $y_i(t)$ (Figure 1). The non-linear parameters related to the resonance frequency shift α is obtained from a simple linear regression fit (Figure 2):

$$\frac{\tilde{f}_0 - \tilde{f}_i}{\tilde{f}_0} = \alpha \cdot A_i \quad (1)$$

$$A_i = \max|Y_i(f)| \quad (2)$$

$$\tilde{f}_i = \max_f|Y_i(f)| \quad (3)$$

Where A_i is the is the peak amplitude of the spectrum, $\tilde{f}_i$ is the peak frequency and $\tilde{f}_0$ denotes the intersection with y-axis of the linear relationship between the peak amplitudes A_i (x-axis) and the peak frequencies $\tilde{f}_i$ (y-axis).

The NIRAS technique obtains the parameter α_f^{NIRAS}, among others, as an indicator of the no linear behavior of the material: the greater the damage, the greater the no-linear behavior and the greater α_f^{NIRAS}.

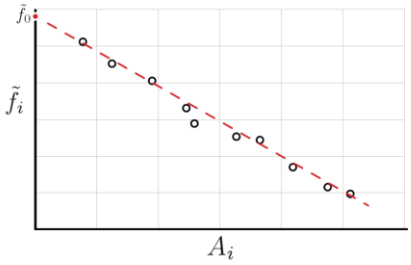

Figure 2. Linear regression from the different resonance signals.

3. EXPERIMENTAL

3.1 Manufacturing and damage induction of mortar specimens

Three mortar specimens (A, B and C) were prepared by mixing Portland cement (EN 197-1-CEM I 52.5 R) [13], sand (quartz) and water in the 1:3:0.5 ratio. After mixing the components, following the procedure described in UNE-EN 196-1 [13], the fresh mortar was placed in a prismatic mold of 50x60x240 mm size. Because prior to pouring the mortar, several optic fibers were settled according to Figure 4. Due to the fragility of the fibers, the mortar was poured in three layers,

avoiding damaging the fibers. For this, the fresh mortar was dropped in a zone free of fiber and then the mold was vibrated (Vibrating Table ToniVIB Tonitechnic) for 30 seconds (vibration frequency 50 Hz, amplitude 1 mm). This procedure was twice repeated and finally the superior part was flattened using a spatula. Additionally, metallic capillary sheath (Figure 3a) was used to protect each optical fiber during the pouring and vibration process and was removed immediately after the surface leveling.

The mold was put in a humid chamber (20 ºC, RH>90%) for 24 hours. After this period, the specimens were carefully demoulded and were covered with a plastic film, to avoid water evaporation. The wrapped specimens were stored in the same humid chamber for 46 days, to complete the hydration of the Portland cement.

After 88 days from mixing the mortar components, two of the specimens were subjected to thermal shock (B and C): the specimens were immersed in hot water (80ºC) for 1 hour and then immediately submerged in cold water (4ºC) for 10 minutes, tank of 0.01 m3.

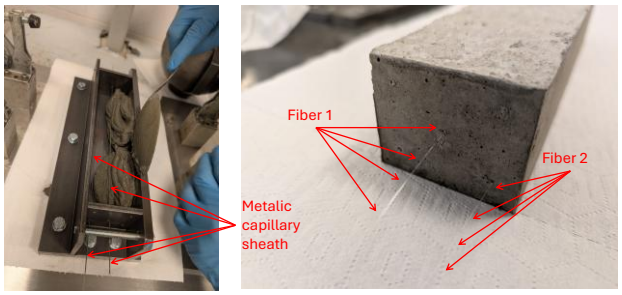

Figure 3. a) Manufacturing process b) Demolded specimen showing the optical fiber emerging from the mortar.

3.2 Embedded Instrumentation

Two of the three specimens (A and B) were internally instrumented during the fabrication process with two optical fibers aligned along the longitudinal axis of the specimen: one positioned at the center and the other near a corner (Figure 4). Each optical fiber contained two integrated Fiber Bragg Gratings (FBGs), which were located at the center and at one end of the fiber.

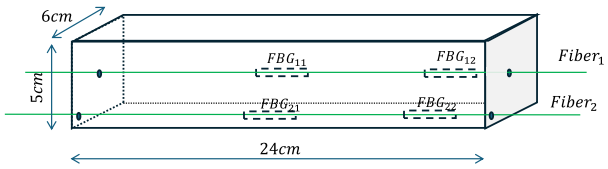

Figure 4. Representación de las fibras embebidas.

The FBGs were primarily tuned to the wavelengths listed in Table 1 and illustrated in Figure 5. Fiber 2 of Mortar A was damaged during the demolding process, therefore no measurements were obtained from this fiber.

Table 1. Wavelengths of the FBGs (nm)

Specimens	$Fiber_1$		$Fiber_2$	
	FBG_{11}	FBG_{12}	FBG_{21}	FBG_{22}
Mortar A	1533.98	1544.05	-	-
Mortar B	1534.07	1543.94	1553.95	1563.80

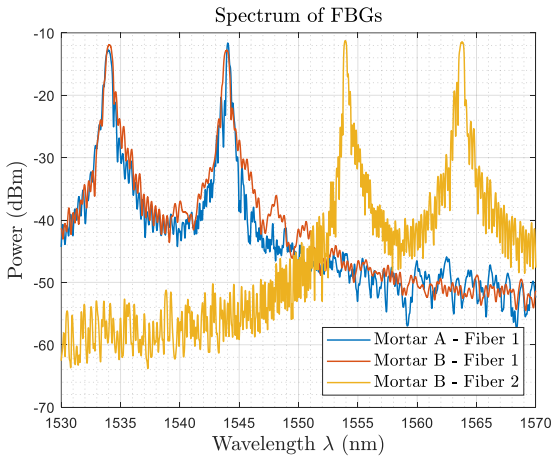

Figure 5. Spectrum of embebed fibers

3.3 Measurement setup

The experimental system employed for the execution of the test comprises three main subsystems: the excitation stage, the sensing stage, and the data acquisition stage.

In the excitation stage, an instrumented hammer was employed to apply controlled impacts to the specimen. The specimen was securely fixed using a custom-designed

support structure. As the hammer remained coupled to the support, multiple measurements could be performed without significant variation in the direction of the impacts, thereby ensuring the repeatability of the excitation conditions.

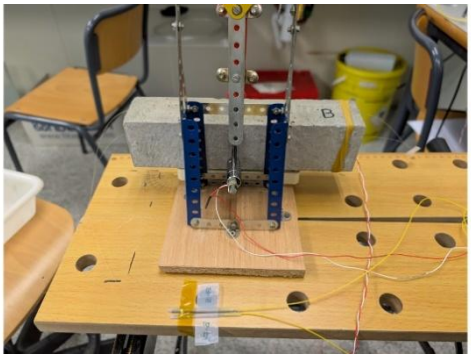

Figure 6. Photograph of the experiment

During the sensing stage, two accelerometers were utilized: one integrated into the instrumented hammer and another attached to the specimen. These devices were employed to record the accelerations induced in both the excitation element (Figure 8 - Column 1) and the tested specimen (Figure 8 - Column 2) . Additionally, two optical fibers were embedded within the specimen. Each fiber contained two Fiber Bragg Gratings (FBGs): one positioned at the center of the embedded section and the other at one of its ends. This configuration enabled the simultaneous monitoring of strain at various critical points of the specimen, with high sensitivity and spatial resolution (Figure 8 - Column 3 and 4). While two optical fibers (fiber 1 and fiber 2) were embedded into the mortar specimens, the present work reports results from only one of them.

The data acquisition stage was performed using two specialized instruments. Accelerometer signals from both the impact hammer and the specimen were recorded using a TiePie HS6 data acquisition system, noted for its high resolution and real-time capture capabilities. For the signals originating from the embedded optical fibers, an optical interrogator manufactured by SENTEA was used. This device features four independent channels and a maximum sampling frequency of 23 kHz. This configuration enabled the simultaneous interrogation of all the Fiber Bragg Gratings (FBGs), with one channel allocated per optical fiber. Each channel allows concurrent reading of multiple FBGs, thereby enabling synchronized acquisition of the two FBGs embedded in each fiber. This is illustrated in Figure 8, where the simultaneous signals from the accelerometers and spatially separated FBGs are plotted.

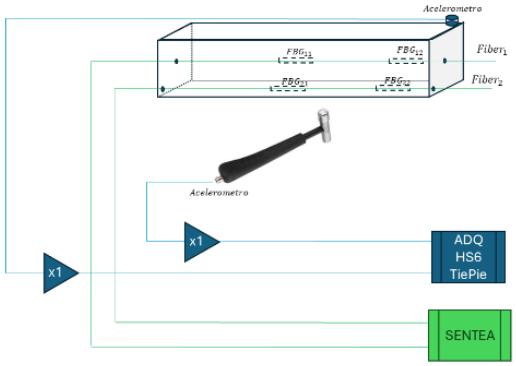

Figure 7. Experimental setup diagram

3.4 Tests description

The tests consisted of applying a series of controlled impacts to the specimen using the instrumented hammer. Each series involved ten consecutive impacts, with increasing force determined by the progressive increase of the striking angle. Upon completion of the first series, the procedure was repeated under similar conditions, applying an additional ten impacts to assess the repeatability of the specimen's dynamic response in its initial (undamaged) state.

As an illustrative example, Figure 8 displays a series of five impacts, showing the signals captured by both the hammer-mounted accelerometer and the surface-mounted accelerometer, as well as the signals recorded by the embedded FBGs in specimen B. The figure clearly shows the proper synchronization and simultaneous acquisition across the different sensor types. The FBG signals exhibit a baseline offset related to the specific wavelength at which each grating is fabricated. This baseline is inherent to the interrogation process itself and this mean value was subtracted from the FBG signals to ensure accurate analysis.

Subsequently, the specimen was subjected to a damage-inducing process via thermal shock. Once its structural properties had been altered, the two-testing series were repeated: ten impacts with the specimen in a non-conditioned state (i.e., without post-damage adjustments), followed by another ten impacts after conditioning. This procedure enabled a comparative analysis of the specimen's

dynamic behavior before and after thermal damage. The experiments are summarized in Table 2.

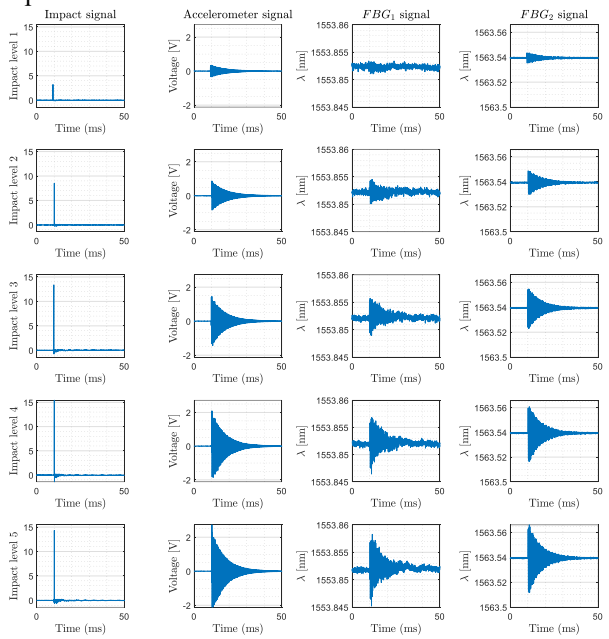

Figure 8. Temporal signals corresponding to different impact levels (displayed in rows) and different sensors (displayed in columns). The signals were acquired from Mortar B - Fiber 2, in its sound state.

Table 2. List of damaged and undamaged mortar samples tested with accelerometers and FBGs.

Sample	Status	Accelerometer	FBG
A	Sound	√	√
	Damage	Reference sample - no damage applied	
B	Sound	√	√
	Damage	√	√
C	Sound	√	No instrumented
	Damage	√	

4. RESULTS

Each experiment comprises ten different impact levels. For each impact signal, a Fourier transform was applied, resulting in a dataset of ten pairs of maximum amplitudes and their corresponding frequencies per experiment.

As an example, Figure 9 presents the normalized amplitudes versus the associated frequencies for specimen B under different conditions (sound and damaged) and using different types of sensors (accelerometers and FBGs). The figure reveals similar trends between the measurements obtained from the accelerometers and the FBGs for the same damage state.

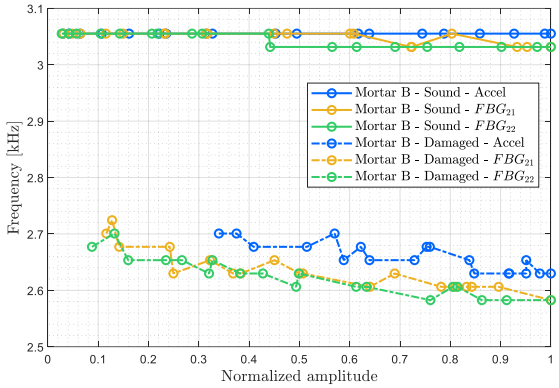

Figure 9. Normalized amplitudes vs frequencies for different conditions (sound and damaged) and different sensor types (accelerometers and embedded sensors FBGs) of specimen B.

From these curves, the NIRAS parameters α_f^{NIRAS} and f_0 were extracted for all the cases, as shown in Table 3. When available, the coefficient of determination R^2 is also reported to assess the goodness of fit. As observed, in the absence of damage, the frequency variation with impact level is negligible, resulting in a very small α parameter as expected for a horizontal line. Additionally, the estimation shows considerable variability, as reflected in the corresponding R^2 values in Table 3.

As damage increases, the nonlinearity in the system's response also increases, which is reflected by a higher α value. In such cases, the linear fit improves significantly. Notably, there is a strong correlation between the results from the accelerometers and the FBG sensors. The advantage of FBGs lies in their ability to accommodate multiple sensing points along the same optical fiber and enable simultaneous interrogation.

In this context, the parameter f_0 serves as a reliable damage indicator because all specimens share the same composition. However, for specimens with different mix proportions (and consequently different f_0 values), the variation in α becomes a more effective indicator of damage presence.

Table 3. NIRAS parameters obtained for different conditions (sound and damaged samples) and different sensor types (accelerometers and embedded sensors (FBG))

	Sound	Damaged
Accel.	**Probes A + B**	**Probes B+C**
$-\alpha$	1.15 ± 3.12	119 ± 20
$f_0\ [kHz]$	3.05 ± 0.003	2.78 ± 0.05
R^2	-	0.72 ± 0.13
$\boldsymbol{FBG_1}$	**Probes A + B**	**Probes B**
$-\alpha$	12.4 ± 17	112 ± 1.4
$f_0\ [kHz]$	3.06 ± 0.003	2.69 ± 0.002
R^2	-	0.76 ± 0.0006
$\boldsymbol{FBG_2}$	**Probes A + B**	**Probes B**
$-\alpha$	29.92 ± 2.1	112 ± 4.40
$f_0\ [kHz]$	3.05 ± 0.003	2.68 ± 0.05
R^2	0.53 ± 0.18	0.80 ± 0.07

5. CONCLUSIONS

This study highlights the potential of embedded sensor technologies as a reliable and effective approach for structural health monitoring in cement materials. In this case, thermal shock has been applied to mortar samples to generate damaged samples. The results indicate that the obtained values from the embedded Fiber Bragg Gratings (FBGs) sensors are similar to piezoelectric sensors. But embedded sensing systems offer numerous advantages, including real-time monitoring capabilities, high sensitivity to damage evolution, and the possibility of spatial and remote operation over the same optical fiber. Despite these benefits, several challenges remain, including sensor protection during the manufacturing process, ensuring long-term durability of the sensors within harsh environments, and reducing implementation cost.

Overall, embedded sensors represent a promising and evolving solution for advancing the reliability and efficiency of structural health monitoring systems in composite structures.

6. Acknowledgments

Grant PID2020-120262GB-I00 funded by MCIN/AEI/ 10.13039/501100011033

7. REFERENCES

[1] R. A. Guyer, P. A. Johnson, Nonlinear Mesoscopic Elasticity: Evidence for a New Class of Materials, *Physics Today* 52 (4), 30, 1999.

[2] L. D. Landau, E. M. Lifshitz, "Theory of Elasticity, Pergamon", Oxford, England, 3rd edn., 1986.

[3] L. Ostrovsky, P. A. Johnson, "Dynamic nonlinear elasticity in geomaterials", *Rivista del Nuovo Cimento 24,* 1–46, 2001

[4] P. C. Aïtcin, "Binders for durable and sustainable concrete", *CRC Press*, 2014.

[5] M. Alexander, S. Mindess, "Aggregates in concrete", *CRC Press*, 2010.

[6] Neville, A. M., "Properties of Concrete" (5th ed.). *Pearson Education*, 2011

[7] Eiras, J. N., et al., "Nonlinear Ultrasonic Evaluation of Thermal Damage in Concrete." Cement and Concrete Research, 80, 31–39, 2016

[8] Payan, C., Garnier, V., Moysan, J., & Johnson, P. A.. "Applying Nonlinear Resonant Ultrasound Spectroscopy to Improve Thermal Damage Assessment in Concrete." *Journal of the Acoustical Society of America*, 121(4), EL125–EL130, 2007

[9] C. Payan, et. al., "Probing material nonlinearity at various depths by time reversal mirrors", *Applied Physics Letters* 104 (14), 144102, 2014.

[10] C. Payan, T. J. Ulrich, P.-Y. Le Bas, T. Saleh, M. Guimaraes, "Quantitative linear and nonlinear resonance inspection techniques and analysis for material characterization: Application to concrete thermal damage", *The Journal of the Acoustical Society of America* 136 (2), 537–546, 2014.

[11] H. J. Yim, J. H. Kim, S.-J. Park, H.-G. Kwak, "Characterization of thermally damaged concrete using a nonlinear ultrasonic method", *Cement and Concrete Research* 42 (11), 1438–1446, 2012.

[12] Chen, J., Bharata, R., Yin, T. et al. "Assessment of sulfate attack and freeze–thaw cycle damage of cement-based materials by a nonlinear acoustic technique". *Mater Struct* 50, 105, 2017.

[13] AENOR, "UNE-EN 197-1. Cement. Part 1: Composition, specifications and conformity criteria for common cements.," 2011. [Online]. Available: www.aenor.es

[14] AENOR, "UNE-EN 196-1. Methods of testing cement. Part 1: Determination of strength.," 2018.